High Temperatures-High Pressures, Vol. 47, pp. 153–164
Reprints available directly from the publisher
Photocopying permitted by license only

High pressure synthesis of siderite ($FeCO_3$) and its thermal expansion coefficient

W. Liang[1], L. Chen[1,2], L. Wang[1,2], Y. Yin[1,2], Z. Li[1,2] and H. Li[1]*

[1]*Key Laboratory of High Temperature and High Pressure Study of the Earth's Interior, Institute of Geochemistry, Chinese Academy of Sciences, Guiyang, 550081, China*
[2]*University of Chinese Academy of Sciences, Beijing, 100049, China*

Received: December 13, 2016; Accepted: March 31, 2017.

In order to study the thermal property of siderite ($FeCO_3$) further, high purity siderite ($FeCO_3$) was artificially synthesized by a simple solid reaction under high temperature and high pressure. The properties of the as-synthesized siderite were investigated by X-ray powder diffraction and Raman spectroscopy, respectively. To find out the siderite stability region of a Pressure-Temperature (P-T) phase diagram, a high pressure synthesis was performed at various conditions, and in this case the principle of siderite synthesized under high pressure was strictly interpreted. The size of micro-particles observed from Scanning Electron Microscope (SEM) image exceeds to 20 micrometers and the Fe content was quantified by Electron Probing analysis. As a typical and important Fe-bearing carbonate mineral, its thermal property is investigated by Thermogravimetric (TG) analysis and high temperature powder XRD refinement, and the thermal expansion coefficient along c-axis ($\alpha_c = 7.995 \times 10^{-6}$/°C), the thermal expansion coefficient along the a-axis ($\alpha_a = 3.313 \times 10^{-6}$/°C) and the volumetric thermal expansion coefficient ($\alpha_V = 1.47 \times 10^{-5}$/°C) was calculated.

Keywords: Siderite, high pressure synthesis, thermal expansion coefficient

1 INTRODUCTION

The interest in carbonate minerals has grown significantly because the global carbon cycle has been a subject of great concern recently and the deep carbon cycle is quite important in the research fields of geophysics

*Corresponding author: liheping@vip.gyig.ac.cn

and geochemistry [1–2]. In the interior of the earth, especially in the lower mantle environment, carbon exists mainly in the form of carbonate, iron carbides, carbon-bearing fluid, diamond, etc. Among these carbon-bearing minerals, magnesite ($MgCO_3$) has been reported to be stable under the temperature and pressure conditions of the earth's lower mantle and it is clear from the previous study that magnesite and siderite can form a complete solid solution ferromagnesite ($Mg_{1-x}Fe_xCO_3$) with rhombohedral structure [3]. Consequently, ferromagnesite could be considered as a carbon host in the interior of the earth [4–5]. It is worth noting that the spin transition of ferromagnesite under high temperature and high pressure can play an important role in the research of elastic properties and wave velocities at lower mantle conditions so as to establish a lower mantle model [6–7].

As an important Fe-bearing mineral, siderite ($FeCO_3$) is the core and the basis for studying the spin transition of ferromagnesite, and also a starting material to synthesize high purity ferromagnesite samples. In particular, the thermal stability of siderite in the environments is the key issue to understand the transfer of crustal carbon into the earth inner through volcanism. Although the properties of natural siderite are well known, the purity siderite deserve further investigation. The natural siderite, which generally exists in sedimentary rock, often forms a solid solution with $MgCO_3$, $MnCO_3$, $CaCO_3$, etc, and those impurities can have a significant effect on the thermal property of siderite. Hence it is necessary to explore methods for artificial synthesis of purity siderite in the laboratory and study its thermal property further.

Due to its very poor heat stability, siderite preparation is very difficult at ambient conditions. In previous studies, siderite synthesis by the hydrothermal method was reported [8]. Although high-purity siderite samples can be obtained by this method, there are still some obvious deficiencies. The micro-particles sizes is too small to satisfy the basic requirement of micro-analysis in geoscience, including micro-constitution and micro-composition analysis. Besides, siderite was also synthesized by solid reaction under high pressure [9]. Furthermore, it is worth considering the more simply process and the high efficiency for siderite artificial synthesis.

In this paper, we report the wide experimental conditions for preparing siderite under high temperature and not very high pressure. The sample was identified by XRD and Raman spectroscopy as siderite single phase without any impurities. Significantly, the crystallinity quality is greatly improved with the micro-particles sizes up to 20–30 micrometers, and the reaction time is controlled within 1h so that the efficiency of the synthesis has been greatly improved. As a typical and important Fe-bearing carbonate mineral, its thermal property is investigated by TG and high temperature XRD and the thermal expansion coefficient was measured.

2 EXPERIMENTS

Using iron oxalate dihydrate ($FeC_2O_4 \cdot 2H_2O$, 99.9%) as the starting material, the sample pellet was made and sealed into a silver capsule of 6 mm in diameter and 3 mm length. Using NaCl as the pressure transmitting medium and graphite as the furnace, high pressure synthesis was performed on a cubic-anvil-type apparatus with the reaction time of 1h. To discuss $FeCO_3$ phase stability region in the P-T phase diagram, the conditions with various pressures and temperatures were used for trial synthesis. Then it was quenched to room temperature and the pressure slowly released. Removing the silver foil from the surface, the sample was obtained.

The property of as-synthesized siderite was investigated by X-ray powder diffraction and Raman spectroscopy respectively, and the result is shown in Figure 1 and Figure 2. The SEM image of as-synthesized siderite microparticles is shown in Figure 3 and the results and details of electron probing analysis are shown in Figure 4 and Table 1. To further explain the synthesis principle of siderite under high pressure, thermogravimetric (TG) analysis was carried out on the starting material $FeC_2O_4 \cdot 2H_2O$ and as-synthesized $FeCO_3$, and the result is presented in Figure 5(a), while a series of samples

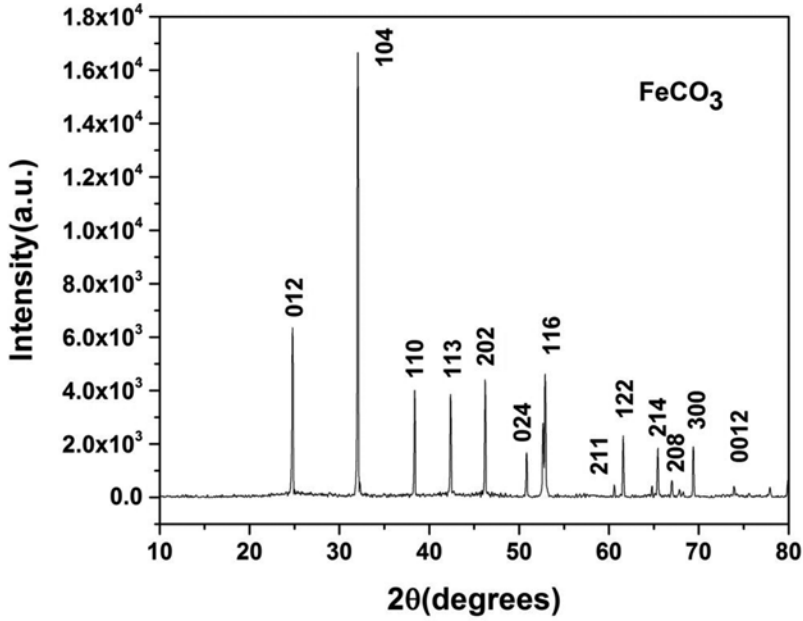

FIGURE 1
The powder XRD of as-synthesized siderite.

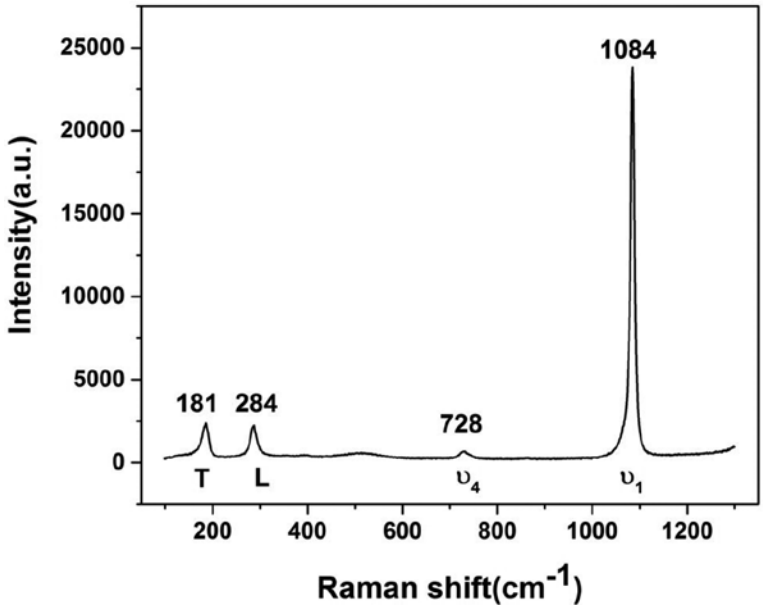

FIGURE 2
Raman spectrum of as-synthesized siderite.

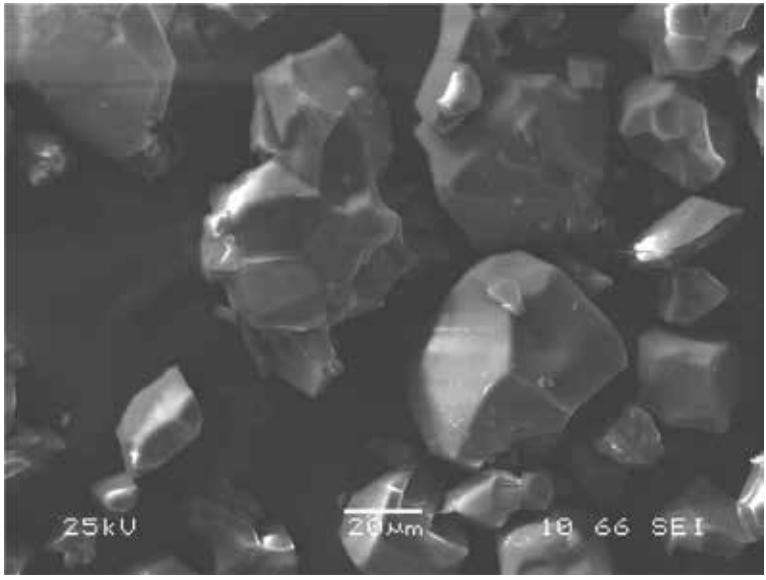

FIGURE 3
The SEM image of siderite.

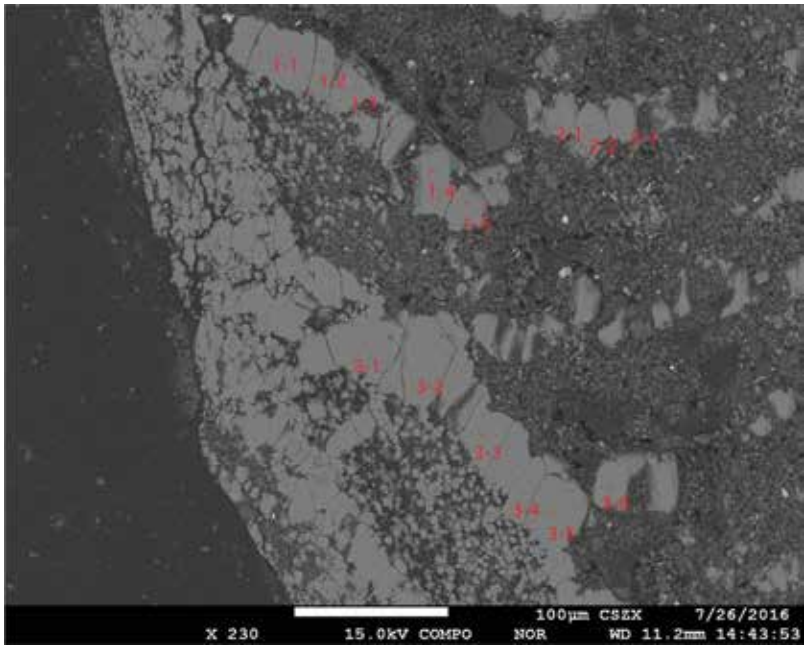

FIGURE 4
The backscattered electronic image of siderite thin section.

TABLE 1
Results of electron probe analysis of as-synthesized siderite

Position No.	Mass fraction of FeO (%)
1–1	61.14
1–2	61.94
1–3	61.33
1–4	61.79
1–5	60.34
2–1	60.64
2–2	62.09
2–3	61.94
3–1	61.22
3–2	61.05
3–3	61.99
3–4	62.16
3–5	61.55
3–6	61.54

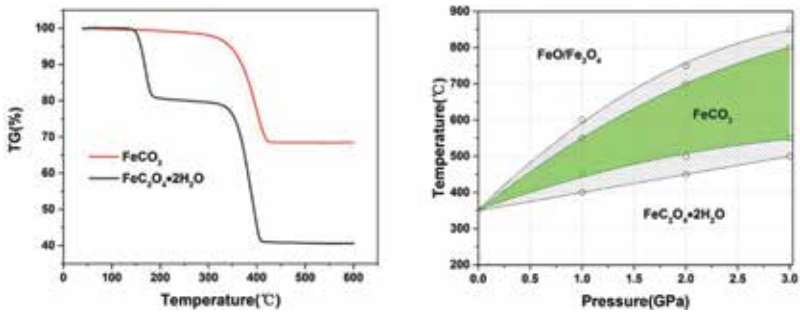

FIGURE 5
(a) TG curves of $FeC_2O_4{\cdot}2H_2O$ with the experimental conditions of argon atmosphere and the rate of temperature rise of 5°C/min. (b) $FeCO_3$ phase stability in the P-T phase diagram.

TABLE 2
Results of assessment phase by high-pressure synthesis from $FeC_2O_4{\cdot}2H_2O$

Experiment conditions	Products (investigated by XRD)
1.0 GPa, 400°C, 1 h	$FeC_2O_4{\cdot}2H_2O$
1.0 GPa, 450°C, 1 h	$FeCO_3$
1.0 GPa, 550°C, 1 h	$FeCO_3$
1.0 GPa, 600°C, 1 h	Fe_3O_4
2.0 GPa, 450°C, 1 h	$FeC_2O_4{\cdot}2H_2O$ & $FeCO_3$
2.0 GPa, 500°C, 1 h	$FeCO_3$
2.0 GPa, 700°C, 1 h	$FeCO_3$
2.0 GPa, 750°C, 1 h	Fe_3O_4 & $FeCO_3$
3.0 GPa, 500°C, 1 h	$FeC_2O_4{\cdot}2H_2O$ & $FeCO_3$
3.0 GPa, 550°C, 1 h	$FeCO_3$
3.0 GPa, 800°C, 1 h	$FeCO_3$
3.0 GPa, 850°C, 1 h	Fe_3O_4 & $FeCO_3$

under various conditions were achieved with the results shown in Table 2. In this way, the stable field of $FeCO_3$ at P-T phase diagram was obtained and the results are shown in Figure 5(b).

High temperature XRD data was collected on a Panalytical multifunction X-ray diffractometer (model: Empyrean), equipped with an Anton Paar high temperature accessory (APHTK-16N). The heating process was performed from ambient temperature to 300°C (below the siderite decomposed tempearture) for 20°C per step in argon atmosphere. Every high temperature step was kept for 10 minutes to ensure temperature uniformity, and 15 XRD

TABLE 3
The result of the parameters of siderite refined from XRD dates at various temperature, where σa, σc and σV is the error bar of the parameters a, c and V, and R^2 is goodness of fit given by Peakfit software.

	a (Å)	**σa (Å)**	**c (Å)**	**σc (Å)**	**V (Å³)**	**σV (Å³)**	**R^2**
25°C	4.69546	0.00014	15.39921	0.00054	294.017	0.017	0.998337
40°C	4.69576	0.00014	15.40076	0.00052	294.084	0.016	0.998647
60°C	4.69617	0.00013	15.40264	0.00054	294.172	0.016	0.998701
80°C	4.69652	0.00014	15.40551	0.00053	294.270	0.017	0.998403
100°C	4.69669	0.00014	15.40734	0.00055	294.326	0.017	0.996832
120°C	4.69714	0.00012	15.40956	0.00054	294.425	0.017	0.994176
140°C	4.69747	0.00014	15.41265	0.00057	294.526	0.017	0.997212
160°C	4.69750	0.00013	15.41629	0.00060	294.599	0.019	0.996329
180°C	4.69812	0.00010	15.41670	0.00060	294.685	0.018	0.995652
200°C	4.69838	0.00014	15.42067	0.00061	294.793	0.020	0.996748
220°C	4.69857	0.00016	15.42318	0.00063	294.865	0.019	0.995857
240°C	4.69875	0.00015	15.42614	0.00069	294.944	0.019	0.995901
260°C	4.69924	0.00016	15.42891	0.00066	295.059	0.020	0.998009
280°C	4.69947	0.00015	15.42969	0.00070	295.102	0.021	0.998144
300°C	4.69989	0.00016	15.43235	0.00072	295.206	0.022	0.998172

patterns were recorded. Using Peakfit and UnitCell XRD analysis software, the crystal structure parameters and unitcell volume have been refined from the high temperature XRD data collected from 25 to 300°C, and the thermal expansion coefficient is calculated and the results was shown in Table 3 and Figure 6.

3 RESULTS AND DISCUSSION

3.1 Powder XRD results

The crystal structure of as-synthesized siderite, which was synthesized at 1.0 GPa and 550°C for 1h, was analyzed by powder XRD as given in Figure 1. All the diffraction peaks can be indexed as the siderite rhombohedral structure. Using silicon (99.999%) as the zero-offset calibration of XRD, all the peaks are fitted with a Lorentzian function. We obtain the structure data of as-synthesized $FeCO_3$ with the space group $R\bar{3}c$ (no.167) and refine the lattice parameters with a = 4.6954(1) Å, and c = 15.3992(5) Å.

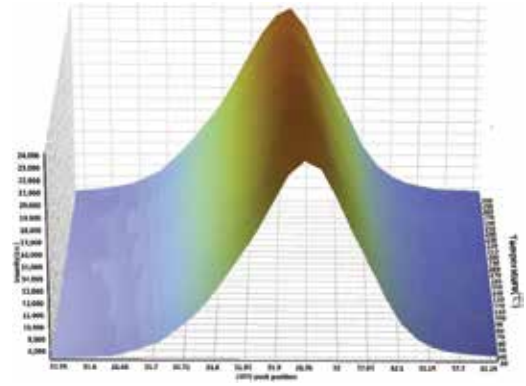

(a)

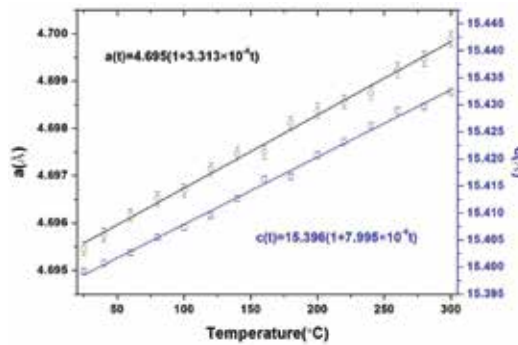

(b)

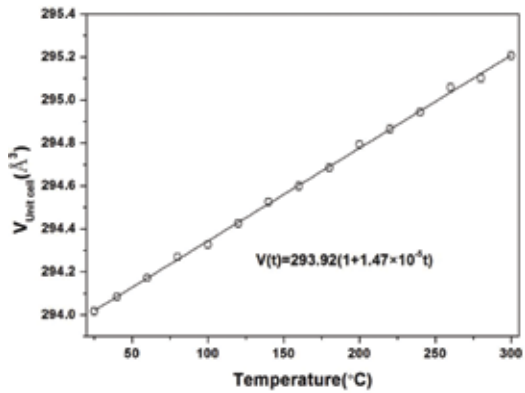

(c)

FIGURE 6
(a) The (104) peaks shift to low angle while siderite heating. (b) The correlation between the parameters of siderite and the temperature. (c) The relationship between the unit cell volume of siderite and the temperature.

3.2 Raman spectrum

The Raman spectrum of the siderite sample, which was prepared at 1.0 GPa and 550°C for 1h is shown in Figure 2. Four Raman active modes in the wavelength range of 100–1300 cm^{-1} were observed located at 181, 284, 728, 1084 cm^{-1}, and all the peak positions were fitted with Lorentz functions. Based on the study of the Raman vibration mode of calcite-type materials including $CaCO_3$, $MgCO_3$, $FeCO_3$, $MnCO_3$, etc. [10–11], these Raman active modes can be described as follows. The peaks at 181 cm^{-1} come from translational lattice mode T. The peak at 284 cm^{-1} is derived mainly from librational lattice mode L. The peak at 728 cm^{-1} is caused by in-plane bending internal mode ν_4. The peak located at 1084 cm^{-1} is caused by symmetric stretching internal mode ν_1.

3.3 Morphology characterization

Figure 3 shows the SEM image of the micro-particles. It can been seen clearly that the as-synthesized siderite consists of the various size of micro-particles and the average size of micro-particles exceeds to 20 micrometers. It makes possible, in this case, to perform the micro-characterization on single micro-particles, such as micro Raman spectrum and electron probing micro-analysis. Subsequently, by controlling the temperature, pressure, reaction time, cooling rate and other experimental conditions, the crystalline grains can be grown further to a larger size, which provides the necessary experimental methods and basis for an attempt at siderite single crystal growth.

3.4 Electron probing analysis

The electron probing analysis was carried out to obtain the micro-composition of the as-synthesized siderite sample. Table 1 shows the Fe content results. Figure 4 shows the back scattering electronic image and the detection position. With Fe_3O_4 as the standard sample of Fe content, we can see from the back scattering electronic image of a thin section siderite sample that the grey scales of the polished surface of all crystalline grains are almost the same. It shows that the samples have almost the same Fe content. A total of 14 points in different areas are selected for probe analysis, and the average mass fraction of FeO obtained is 61.48%. It can be calculated that the sample composition is $Fe_{0.99}CO_3$.

3.5 $FeCO_3$ phase stability in the P-T phase diagram

Through TG analysis and a series of experiments under various temperature and pressure conditions, $FeC_2O_4{\cdot}2H_2O$ and $FeCO_3$ on a P-T phase diagram was obtained.

Figure 5(a) is a TG curve of $FeC_2O_4{\cdot}2H_2O$ and $FeCO_3$, which adopts argon atmosphere to protect the Fe^{2+} with the conditions of the rate of temperature rise 5°C/min. It can be seen clearly from the TG that a decomposition reaction will occur with both $FeC_2O_4{\cdot}2H_2O$ and $FeCO_3$ when the temperature is in

the range of 300–400°C. Thus $FeCO_3$ cannot be obtained through decomposition of $FeC_2O_4{\cdot}2H_2O$ directly.

In comparison, high pressure can greatly improve the thermal stability of $FeCO_3$, so that the range of the decomposition temperature of $FeC_2O_4{\cdot}2H_2O$ and $FeCO_3$ separates. In the P-T phase diagram, corresponding temperature T and pressure P can decompose the phase of $FeC_2O_4{\cdot}2H_2O$ and stabilize the phase of $FeCO_3$ so as to successfully synthesize $FeCO_3$. Table 2 shows the reaction products of $FeC_2O_4{\cdot}2H_2O$ under different temperature and pressure conditions. Figure 5(b) shows the stability of $FeC_2O_4{\cdot}2H_2O$-$FeCO_3$ in the P-T phase diagram, in which the decomposition temperature of $FeC_2O_4{\cdot}2H_2O$ and $FeCO_3$ is supposed be to 350°C at ambient pressure. The green region is the phase stability region of $FeCO_3$, and the dashed area is the phase boundary. From the P-T diagram, the decomposition temperature of $FeCO_3$ and $FeC_2O_4{\cdot}2H_2O$ is obviously increasing with the increased pressure. In this case, due to the decomposition temperature of $FeCO_3$ increasing more quickly than $FeCO_4{\cdot}2H_2O$, the stable phase region of $FeC_2O_4{\cdot}2H_2O$ and $FeCO_3$ separates, and the greater pressure is more conducive to the stability phase of $FeCO_3$.

In addition, it is worth noting that the final decomposition product of $FeCO_3$ is Fe_3O_4, not FeO theoretically. In conclusion, FeO is so sensitive to oxygen fugacity that it is unstable in the same oxygen fugacity environment in which $FeCO_3$ can be stable, and it exists in the form of a higher oxidation state Fe_3O_4.

3.6 The thermal expansion coefficient

Many enough data points for temperature step of 20°C were collected from high temperature XRD to ensure an accurate and reasonable result. Though it is observed clearly from Figure 6(a) that the (104) diffraction peaks shift to low angle while heating from 25°C to 300°C, the thermal expansion coefficient of siderite is much smaller than other minerals and in this case the parameters changes so little that the algorithm of refinement software is very important for data accuracy. GSAS is a good software for Rietveld refinement, but it is not very sensible to data accuracy when the temperature point is very close to, which could be caused by the influence of GSAS refinement parameters and functions. Since many attempts involve data accuracy, Peakfit + UnitCell software was used to refine structure parameters [12]. In comparison, it is a direct solution algorithm from Bragg equation and has better accuracy because it avoids the impacts of refinement parameters and functions.

All diffraction peaks were fit with Gaussian + Lorentzian functions by Peakfit software to quantify diffraction angles for every high temperature XRD pattern, in which the goodness of fit was given by R^2. Then input the diffraction peaks position with corresponding hkl into UnitCell software, and calculate the unit cell parameters (a, c and unit cell volume). The unit cell parameters are give in Table 3 and shown in Figure 6(b)(c).

The unitcell parameters show a linear and continuous increase with increasing temperature, and the V-T state equation at 1atm can be fitted with the linear relationship. The thermal expansion α is equal to 1/V dV/dT, and the exponential can be expanded linearly to $V(T) = V(T_0)(1 + \alpha(T\text{-}T_0))$ for small $(T\text{-}T_0)$. When select T_0 value of 273 K, $(T\text{-}T_0)$ is equal to centigrade temperature t, and the linear relationship between the unit cell parameters and temperature can be fitted as follows,

$$a(t) = 4.695(1 + 3.313 \times 10^{-6}t),\ \alpha_a = 3.313 \times 10^{-6}/°C$$
$$c(t) = 15.396(1 + 7.995 \times 10^{-6}t),\ \alpha_c = 7.995 \times 10^{-6}/°C$$
$$V(t) = 293.92(1 + 1.47 \times 10^{-5}t),\ \alpha_V = 1.47 \times 10^{-5}/°C$$

The calculation of axial thermal expansivity exhibits an obvious anisotropy and indicates that the thermal expansion coefficient along c-axis ($\alpha_c = 7.995 \times 10^{-6}/°C$) is over two times more than the a-axis ($\alpha_a = 3.313 \times 10^{-6}/°C$). In addition, the volumetric thermal expansion coefficient is also calculated with $\alpha_V = 1.47 \times 10^{-5}/°C$. The value of volumetric thermal expansion coefficient we obtained is much smaller than the results of natural siderite ($Fe_{0.95}Mn_{0.045}Mg_{0.005}CO_3$, $\alpha_V = 6.44 \times 10^{-5}/°C$) [13], and the difference could be caused by Mn^{2+} and Mg^{2+} impurities.

4 CONCLUSION

The thermal expansion coefficient of impurity-free siderite was quantified by high temperature XRD at ambient pressure. The crystallinity quality is improved with the micro-particle size up 20 micrometers, which could provide bases for siderite single crystal growth. The high temperature and high pressure research in its spin transition, including P-V-T equation of state and high pressure Raman spectroscopy, can be carried out in the future.

ACKNOWLEDGEMENTS

We thank Yong Meng (Institute of Geochemistry, Chinese Academy of Sciences, Guiyang) for his valued assistance. This work was financially supported by 135 Program of the Institute of Geochemistry (Y2ZZ041000), CAS, the National Key Research and Development Plan (2016YFC0600100), and Large-scale Scientific Apparatus Development Program (YZ200720), CAS.

REFERENCES

[1] Hazen R. M., Hemley R. J., Mangum A. J., Eos,Transactions, American Geophysical Union. 93 (2012), 17–18.
[2] Keppler H., Wiedenbeck M., Shcheka S. S., Nature, 424 (2003), 414–416.

[3] Rosenberg P. E., American Mineralogist, 48 (1963), 1396–1400.
[4] Isshiki M., Irifune T., Hirose K., Ono S., Ohishi Y., Watanuki T., Nishibori E., Takata M., Sakata M., Nature, 427 (2004), 60–63.
[5] Oganov A. R., Ono S., Ma Y., Glass C. W., Garcia A., Earth and Planetary Science Letter, 273 (2008), 38–47.
[6] Lin J-F, Tsuchiya T., Physics of the Earth and Planetary Interiors, 170 (2008), 248–259.
[7] Lavina B., Dera P., Downs R. T., Prakapenka V., Rivers M., Sutton S., Nicol M., Geophysical Reasearch Letter, 36 (2009), L23306.
[8] Chai L., Navrotsky A., Geochimica et Cosmochimica Acta, 60 (1996), 4377–4383.
[9] Cerantola V., McCammon C., Kupenko I., Kantor I., Marini C., Wilke M., Ismailova L., Solopova N., Chumakov A., Pascarelli S., Dubrovinsky L., American Mineralogist, 100(2015), 2670–2681
[10] Rividi N., van Zuilen M., Philippot P., Menez B., Godard G., Poidatz E., Astrobiology, 10 (2010), 293–308.
[11] Herman R. G., Bogdan C. E., Sommer A. J., Simpson D. R., Applied Spectroscopy, 41(1987), 437–440.
[12] Holland T. J. B., Redfern S. A. T., Mineralogical Magazine, 61(1997), 65–77.
[13] Merlini M., Sapelli F., Fumagalli P., Gatta1 G. D., Lotti P., Tumiati S., Abdellatief M., Lausi A., Plaisier J., Hanfland M., Crichton W., Chantel J., Guignard J., Meneghini C., Pavese A., Poli S. American Mineralogist. 101 (2016), 1423–1430.